Intraspecies warfare restricts strain coexistence in human skin microbiomes

Christopher P. Mancuso[1,2], Jacob S. Baker[1,2], Evan Qu[1,2], A. Delphine Tripp[1,2,3], Ishaq O. Balogun[1,2], Tami D. Lieberman[1,2,4,5] *

1 Institute for Medical Engineering and Sciences, Massachusetts Institute of Technology; Cambridge, MA 02142, USA.
2 Department of Civil and Environmental Engineering, Massachusetts Institute of Technology; Cambridge, MA 02142, USA.
3 Department of Systems Biology, Harvard University; Cambridge, MA 02138, USA.
4 Broad Institute of MIT and Harvard; Cambridge, MA 02142, USA.
5 Ragon Institute of MGH, MIT, and Harvard; Cambridge, MA 02142, USA.

* Corresponding author: tami@mit.edu

Abstract

Determining why only a fraction of encountered or applied bacterial strains engraft in a given person's microbiome is crucial for understanding and engineering these communities[1]. Previous work has established that metabolism can determine colonization success *in vivo*[2–4], but relevance of bacterial warfare in preventing engraftment has been less explored. Here, we demonstrate that intraspecies warfare presents a significant barrier to strain transmission in the skin microbiome by profiling 14,884 pairwise interactions between *Staphylococcus epidermidis* cultured from eighteen human subjects from six families. We find that intraspecies antagonisms are abundant; these interactions are mechanistically diverse, independent of the relatedness between strains, and consistent with rapid evolution via horizontal gene transfer. Ability to antagonize more strains is associated with reaching a higher fraction of the on-person *S. epidermidis* community. Moreover, antagonisms are significantly depleted among strains residing on the same person relative to random assemblages. Two notable exceptions, in which bacteria evolved to become sensitive to antimicrobials found on the same host, are explained by mutations that provide phage resistance, contextualizing the importance of warfare among other lethal selective pressures. Taken together, our results emphasize that accounting for intraspecies bacterial warfare is essential to the design of long-lasting probiotic therapeutics.

Main

It is now clear that new strains are acquired throughout life in the gut[5,6], oral[6], vaginal[7], and skin[8,9] microbiomes. Despite this potential for transmission, the microbiomes of cohabitating adults do not homogenize[10], with each individual harboring person-specific strains[11]. Neutral priority effects[12,13], such as competition with established strains for metabolic[4,14] or spatial niches[15,16], have been explored as potential drivers of person-specificity. Alternatively, selection for specific species or strains could be driven by the immune system[17,18], host behavior (e.g. diet[19] or hygiene[20]), or other members of their microbiome[21].

Intraspecies warfare has been underexplored as a source of person-specific selection and barriers to strain colonization. Bacteria often actively antagonize other bacteria— from the same[22] or different[23] species— through a variety of contact-dependent and contact-independent mechanisms[21,24]. Both antimicrobial production and resistance can vary within species, often changing quickly through horizontal-gene-transfer[25–27]. To date, most work on interbacterial warfare in microbiomes has focused on antagonisms between different species[28–30] and its potential to provide colonization resistance against pathogens[23,31]. However, given that niche overlap is highest within a species[32], the selective advantage

for inhibiting competing microbes is expected to be strongest when the competitor is from the same species[30,21,24].

Here, we leverage *Staphylococcus epidermidis* in the facial skin microbiome as an ideal system for studying barriers to strain transmission. Each person's facial skin microbiome is typically colonized by several strains of *S. epidermidis* arising from distinct colonizing genotypes[9,16], with cohabitating individuals retaining unique compositions[9]. *S. epidermidis* is known to produce a variety of interspecies antimicrobials[33,34], and the accessory genome harbors an enrichment of antagonism-related biosynthetic gene clusters (BGCs) and defense genes (Supplementary Figure 1; Methods). Physical barriers to transmission are expected to be low for surface-dwelling microbes, necessitating an explanation for the person-specificity of these intraspecies communities.

To test if intraspecies warfare is a major barrier to *S. epidermidis* strain colonization, we examined antagonistic interactions among a collection of *S. epidermidis* isolates collected from extensively-sampled, nuclear family members[9]. Ecologically-relevant warfare should result in fewer antagonisms between strains on a person than expected by random assembly of available strains (Figure 1A).

Leveraging a collection of 1,870 sequenced *S. epidermidis* isolates from 18 people from 6 families, from which we also have metagenomic data[9], we built a library of 122 isolates that capture genomic diversity on these individuals. This library includes 59 lineages, clusters of isolates separated less than 100 point mutations across their entire genomes[9]. Of these, 30 lineages were shared between family members and 29 lineages were unique to an individual. We also included 23 isolates of other skin bacterial species incidentally isolated from the same subjects. This library reflects ~96% of the *S. epidermidis* relative abundance on these people (Supplementary Figure 2)[9], enabling efficient estimation of antagonism frequencies.

We conducted high-throughput solid-phase competition assays ("spot-on-lawn"[35]) to assess toxin production and sensitivity for each of 21,025 pairwise combinations of isolates (Figure 1B). For each isolate, we made a bait lawn by embedding cells into soft agar. We then grew the full library to mid-log phase in liquid media, spotted aliquots on top of bait lawns at high cell density, and allowed cells to grow until the bait lawns were opaque (Methods). A zone of inhibition (ZOI) was observed around ~7% of spots, indicating the bait's sensitivity to an antimicrobial produced by the spot (Figure 1C). We quantified the presence and size of ZOIs computationally, enabling detection of even weak inhibition (Figure 1D).

Antimicrobials are diverse and fast-evolving

Interactions are generally conserved at the lineage level but display no longer-lasting phylogenetic structure. Only 3.1% and 3.4% of possible interactions showed intra-lineage variation in antagonism or sensitivity, respectively (Supplementary Figures 3 and 4), suggesting minimal recent on-person evolution of antimicrobial production or resistance.

However, at broader within-species levels, antagonism is broadly distributed across the phylogeny with no apparent clustering (Figure 2A) or correlation with sequence similarity ($P > 0.144$, permutation test; Supplementary Figure 5). Four "super-antagonizer" lineages are responsible for 62% of the antagonisms and 44% of isolates antagonize at least one lineage. We observe no significant difference between frequencies of interspecies and intraspecies antagonism when accounting for

structure in the interaction matrix ($P = 0.574$, permutation test; Figure 2B; Methods); moreover, some antagonists participate in both intra- and inter-species killing. There was also no difference in antagonism whether lineages used the same or different quorum sensing variant (agr type, $P = 0.256$, permutation test, Figure 2C), suggesting that intraspecies communication is not a major determinant of sensitivity. These observations indicate that it may be impossible to predict production or sensitivity to intraspecies antimicrobials using higher-order phylogenetic signals or single marker genes.

The wide variety of interaction patterns observed suggests a diverse pool of antimicrobial molecules. For 20 isolates chosen based on the abundance and diversity of interaction patterns (Supplementary Figure 6; Methods), we repeated screening using filtered culture supernatants that were either treated with heat, proteinase-K, removal of small molecules by desalting, dilution, or not treated (Figure 2D, Supplementary Figure 7A, and Supplementary Table 2). We also repeated spot-testing to test for iron-suppression[34] (Supplementary Figure 7B; Methods). Together, these results suggested a wide variety of competitive mechanisms, including peptides, iron-chelators, and other proteins (Fig. 2E). Importantly, super-antagonizers had different mechanisms of interaction, with one showing a pattern indicative of multiple effector types (Supplementary Figure 7C).

While antagonist lineage genomes contain a variety of potential biosynthetic clusters (BGCs) for known and unclassified products (Supplementary Table 3), not all isolates with the same BGC had the same interactions, indicating the presence of multiple BGCs per isolate, the incomplete expression of all BGCs, or both. Moreover, not every antagonist had a clearly identified BGC, highlighting the likelihood that new classes of antimicrobials remain to be discovered.

On-person depletion of warfare

To test for ecological relevance of these antimicrobial interactions, we looked to see if antagonistic interactions were depleted among lineages present on a same person at a single timepoint, relative to randomly chosen lineages. We assessed the Antagonism Frequency (AF) for each sample, a metric that accounts for lineage abundances ($AF = \sum_{i,j} f_i f_j I_{ij}$ where f represents the frequency of that lineage in that sample and $I_{ij} = 1$ if lineage i antagonizes lineage j; see Methods). While AF for the collection as whole is ~15%, we find that the majority of samples have AF values of zero and an overall significantly lower distribution of AF across samples than expected ($P < 0.001$, one-sided t-test; Figure 3A). Antagonisms remain depleted if each subject or family is counted just once, using mean AF across samples ($P = 0.017$ and $P = 0.012$, respectively, one-sided t-test; Supplementary Figure 9A-C).

Rather than assume a random interaction matrix, we applied permutation tests in which lineage labels are shuffled across samples, which confirmed that there is a significant depletion of antagonism ($P = 0.009$, permutation test; Methods; Figure 3B). Additional permutation tests, in which lineage labels are only shuffled within a family, also showed significant depletion of on-person interactions ($P < 0.044$, permutation test; Supplementary Figure 9D-G), further supporting the *in vivo* relevance of these interactions.

The ecological signature of antagonism is easily observable when the interaction network is sorted by subject (Figure 3C). Subjects carrying antagonist lineages have significantly different *S. epidermidis* compositions than their family members, who carry sensitive lineages (Figure 3C). It is also notable that the outlier samples with antagonism between co-resident lineages are mostly samples from children (Figure 3A), whose skin microbiome has lower cell densities[9,36] and higher rates of lineage

turnover[5]. Notably, other assessments of *S. epidermidis* diversity, including quorum-sensing variants[37] or phylogenetic groupings (Supplementary Figure 10), do not display these person-specific, ecological signatures.

This indication of the importance of within-species warfare suggests that antagonistic lineages have increased fitness on human skin relative to non-producing strains. Accordingly, lineages that antagonize many others generally reach higher relative abundances of the *S. epidermidis* community on individual people ($P = 0.004$, $\rho = 0.249$, Spearman Rank Correlation; Figure 3D). However, antagonistic capacity does not correlate with the number of subjects in our cohort a lineage has colonized ($P = 0.004$, Spearman Rank Correlation; Supplementary Figure 12B). Since antagonism provides a selective advantage on individuals, but this does not translate to high prevalence, there must either be tradeoffs in overcoming other colonization barriers (e.g. priority effects) or frequent evolution of resistance undetected in our sampling. We did not find evidence of strong-tradeoffs for production *in vitro*, as producers and non-producers have comparable growth rates ($P = 0.3$, Spearman Rank Correlation; Supplementary Figure 12C); however, this does not rule out the possibility of *in vivo* tradeoffs for production.

On-person evolution of sensitivity

Three outlier subjects (2PA, 2PB, and 5PA) account for 95% of all antagonisms observed between co-resident lineages on adults (Methods). Strikingly, two lineages on these adults were among those with intra-lineage differences in sensitivity, suggesting on-person evolution of resistance or sensitivity. Surprisingly, the phylogenetic tree structures were indicative of on-person evolution of sensitivity from a resistant ancestor (Supplementary Figure 10).

Moreover, the two "idiosyncratic" isolates with derived sensitivity (isolate 3 from lineage 20, 20.3; and isolate 3 from lineage 37, 37.3) were vulnerable to the same group of antagonists (Figure 4A). This striking similarity suggests related mechanisms of susceptibility, and we therefore looked for similar mutations acquired by the idiosyncratic isolates. Despite fewer than 100 mutations within each lineage, we found a clear commonality: a nonsense mutation in *vraG* in isolate 20.3 and a frameshift in *vraF* in isolate 37.3 (Supplementary Figure 10). Deletions in the *vraFG* signal-transduction complex[38] or its downstream pathways[39,40] are known to increase sensitivity to cationic antimicrobials produced by bacteria and humans; these mutations suppress modifications to wall-teichoic acid (WTA)[40] and phosphatidylglycerol[39] that increase cell envelope charge. Consistent with this expectation, idiosyncratic isolates were more sensitive to the cationic, but not mildly charged, antimicrobials we tested (Figure 4B, Supplementary Figure 12). Idiosyncratic isolates also had increased sensitivity to lysostaphin, an enzyme targeting the cell wall (Figure 4B).

To confirm the causative role of *vraFG* mutations driving sensitivity, we plated isolate 37.3 on high levels of polymyxin B to select for resistant colonies (Figure 4C; Methods). Two of ten resistant isolates corrected the *vraF* frameshift, and had an ancestral resistance profile (see isolate 37.3-r1; Figure 4B). These results confirm that the observed sensitivity was driven by *de novo* mutations acquired on individuals that break the *vraFG* pathway.

The parallelism between the two lineages strongly suggests that the loss of *vraFG* is advantageous on these hosts. Moreover, a second lineage (58) on subject 2PA showed the same pattern of sensitivity (Supplementary Figure 6) and also had nonsynonymous mutations in the same genetic pathway (Supplementary Figure 10). Together, these results raise the possibility that *vraFG* loss creates

a tradeoff between warfare sensitivity and some other, advantageous, phenotype. The benefit of these mutations is not faster growth: the *vraF* mutant 37.3 grows slower than its full-length *vraF* revertant 37.3-r1 (Supplementary Figure 12C).

What tradeoff might remain that provides an advantage for *vraFG* loss? Cell envelope modifications often affect phage susceptibility, including multiple WTA-modifications recently characterized in *Staphylococci*[41,42]. We applied phage-containing supernatant obtained in our mechanism screen (from isolate 32.1; Methods) and quantified plaque-forming-units (PFU). We obtained 6x fewer PFU on *vraF* mutant 37.3 than revertant 37.3-r1 ($P < 0.001$, one-sided t-test; Figure 4D), consistent with increased phage resistance. We did not obtain any plaques on isolates from lineage 20 or 58, potentially due to other resistance mechanisms[43] against the tested phage. While we were unable to isolate phage directly from swab samples from subjects with idiosyncratic isolates (Methods), these results together suggest that similar phages may have existed on these subjects, driving parallel selection for cell envelope modification at a cost of sensitivity to cationic antimicrobials (Figure 4E).

Discussion

Here we show that interbacterial warfare plays a critical role in determining commensal survival on human skin. These observations reconcile the accessibility of the skin to new *S. epidermidis* colonizations[9] with the person-specific nature of strain composition[8,44,37,9].

Given the advantage that warfare seems to confer, why don't "super-antagonists" -- or "super-resisters" -- dominate the global population? While the potential reasons are numerous and complex, our results point to the existence of selective tradeoffs for antimicrobial resistance; such tradeoffs may also exist for production of different weapons. Antimicrobial exporters and cell envelope components could be targeted by phage[42] and the immune system[18,45], imposing harsh selective pressures against antagonists and resistors on certain hosts. Priority effects[12,13], selection on orthogonal phenotypes[4,46], and fitness deficits induced by the cost of production may also play important roles, though we find no consistent growth deficit for production or resistance here.

This evidence of *in vivo* exclusion by antagonists suggests strain mixing at length scales over which antimicrobials can act. *S. epidermidis* is generally thought to live on the surface of skin[47] and mix with other strains and species; however, the fine-scaled spatial structure of *S. epidermidis* on skin remains to be explored. Determining whether strains are evenly mixed or only compete at the borders of small, overlapping clonal patches will require the application of additional sampling[48] or imaging methods[49].

While other studies have identified trends between phylogenetic distance and probability of antagonism[28–30,50], we find no such significant signal here. Instead, our observations are consistent with rapid horizontal gene transfer and molecules that mediate both interspecies and intraspecies warfare; these phenomena both make it difficult to interpret the relationship between phylogenetic distance and antagonism. Whether intraspecies or interspecies[34,33,23,51,52] antagonism provides the primary selective advantage for production is unclear. Given the high metabolic overlap among strains of a species[30,32], it is possible that interspecies killing is simply a byproduct of intraspecies killing. Experiments enabling higher throughput, combined with deep strain profiling from many species on the same set of people, will be required to address the relative roles of intraspecies and interspecies warfare on humans. Regardless our results show that intraspecies warfare contributes to strain composition *in vivo*.

The high turnover of antimicrobial production and sensitivity highlight that whole-genome resolution may be required to predict the ability of a person's microbiome to resist pathogens. However, even given perfect genomic information, understanding the genetic basis of production and resistance will be critical. Particularly given the potential for tradeoffs between resistance to the host[53,54], phage[41], and antimicrobials, the specific mechanisms of resistance will be paramount for predictive modeling. The diversity of antagonistic patterns observed here precludes straightforward association of interactions to genetic elements, highlighting the need for novel approaches to identify and characterize new antimicrobials, BGCs, and resistance determinants[55–58].

Many studies have focused on overcoming metabolic[59] and immune[45] barriers to engraftment in human microbiomes. Our results assert that interbacterial antagonism should be considered alongside these forces when designing microbiome-targeted therapies. Probiotic success may require eliminating pre-existing microbes, confirming resistance to resident toxin-producers, or bet-hedging with multiple probiotic formulations. However, after overcoming these barriers, engrafted probiotics that actively protect their niches could ensure long-lasting therapeutic benefits.

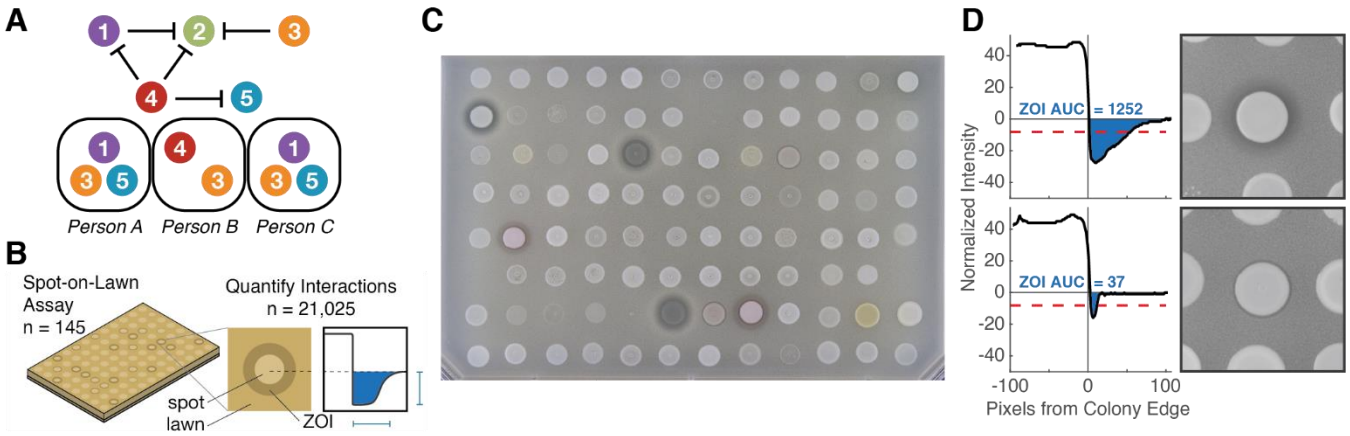

Figure 1: High-throughput assay of interbacterial warfare from skin microbiomes of related people. (A) Antagonism between different commensal strains of the same species (circles) could theoretically prevent transmission of certain strains despite frequent contact between individuals. Ecologically-relevant warfare would result in a depletion of antagonisms on individual people relative to expectation. (B) We built a library of 122 *Staphylococcus epidermidis* isolates representing the strain diversity on healthy individuals from six families, and included 23 isolates from other skin species from these people. We screened every pairwise interaction (14,884 *S. epidermidis* intraspecies interactions plus 6,141 including other species) using high-throughput "spot-on-lawn" assays, in which producer cells are spotted on top of a lawn of receiver cells; we identified hundreds of cases of antagonism, which appear as zones-of-inhibition (ZOIs). (C) Representative photograph of spot-on-lawn assay. Several *S. epidermidis* spots produce antimicrobials that antagonize the *S. epidermidis* receiver lawn, resulting in ZOIs of a range of intensities. (D) We developed a computer-aided image analysis pipeline to identify even subtle ZOIs and quantify the strength of antagonism, determined by the area under the curve of the intensity traces (AUC, blue).

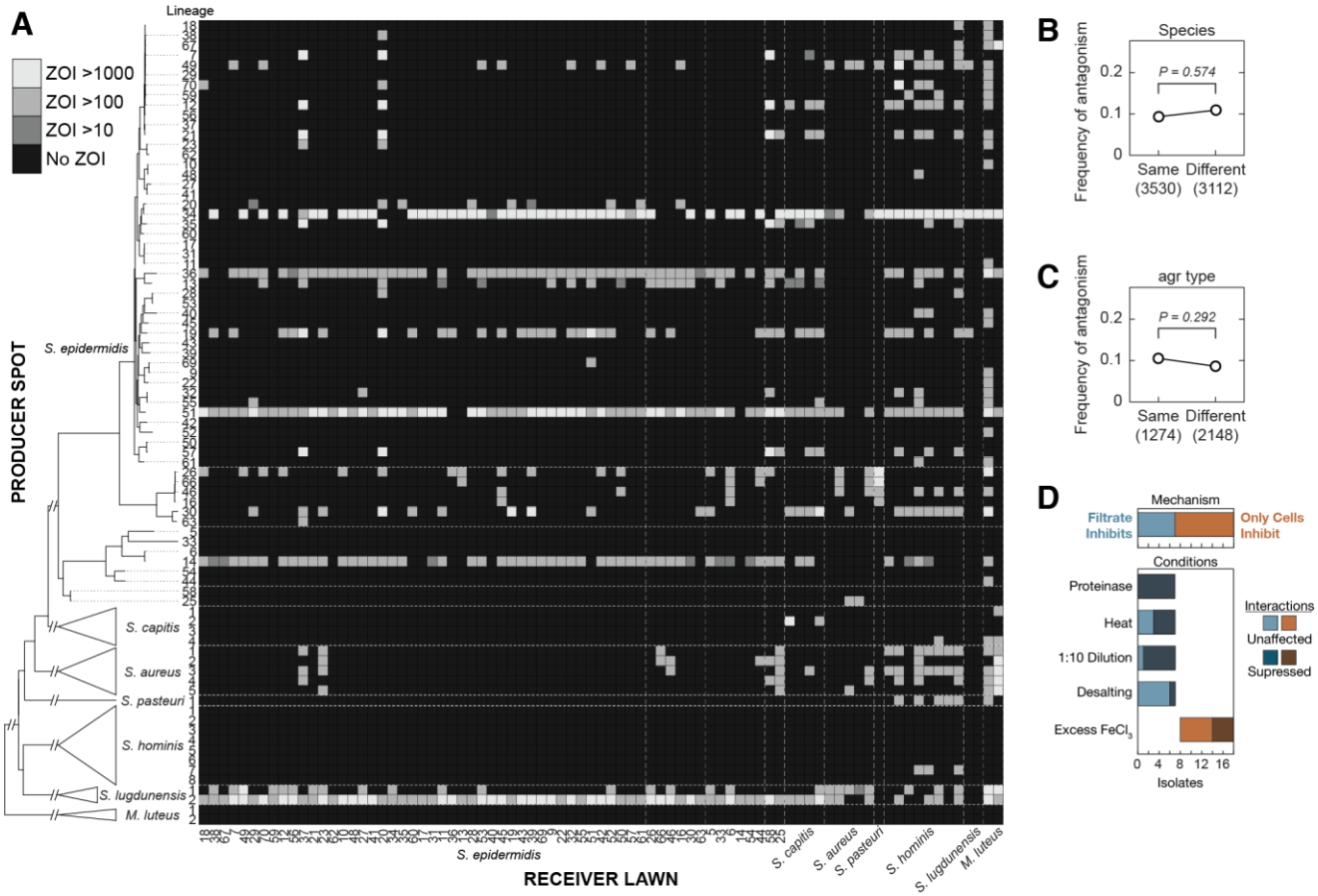

Figure 2: Intra-species antagonism is common and does not segregate at higher phylogenetic levels. (A) The heatmap depicts the Area Under the Curve (AUC) for the Zone Of Inhibition (ZOI) calculated for pairwise interactions between *S. epidermidis* lineages and other skin microbiome isolates. Lineages and species are sorted by phylogenetic similarity (see tree, not to scale), with dashed lines to indicate phylogroup and species boundaries. No structure is observed in the producers (rows) or receivers (columns) of the heatmap, indicating that antimicrobial production and resistance are recently derived. Four *S. epidermidis* lineages are "super-antagonists", inhibiting the majority other tested isolates but differences in their targets indicate distinct mechanisms. (B-C) The frequency of antagonism does not significantly differ between members of the same or different (B) species or (C) quorum sensing variant (agr type). Significance p-values are derived from two-sided permutation tests with shuffled group labels. Altogether, our results show antagonism is not conserved beyond the lineage level and warfare is common among even closely related lineages, consistent with the hypothesized advantage gained by targeting strains with similar niches. (D) To assess the mechanisms of antagonistic interactions, we repeated the screen using cells and filtrates from 20 *S. epidermidis* producers against an array of bait lawns chosen based on interaction profiles (Supplementary Figure 6). Filtrates were subjected to a variety of pre-treatments, whereas cell-based interactions were retested on media containing excess iron to identify iron-suppression. The results obtained suggest a large variety of interaction mechanisms, and are not neatly predictable from genomic context in this size screen (Supplementary Figure 7).

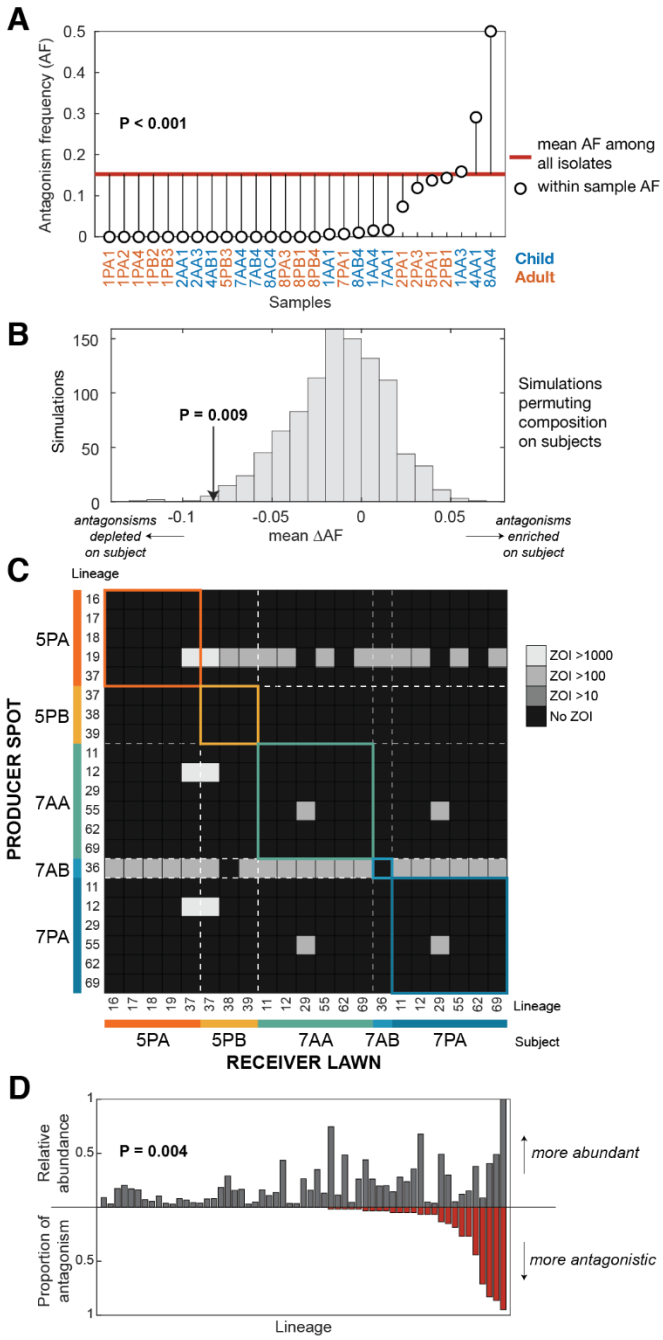

Figure 3: Antagonism is depleted among lineages co-residing on individuals. (A) The frequency of antagonistic interactions between co-resident lineages in samples (e.g. same person, same timepoint) is depleted relative to their frequency across all *S. epidermidis* lineages (red), one-sample t-test. Label color denotes subject age group and sample codes indicate family, subject, and timepoint (e.g. 1PA1 is subject 1PA, timepoint 1). (B) A more realistic null-model, in which the antagonism matrix is kept constant but lineage identities are shuffled across all subjects in our study, also reveals a significant depletion of antagonism in the observed (arrow) antagonism frequency of coexisting lineages on individuals relative to simulations (ΔAF, permutation test). (C) A section of the lineage-level heatmap from Figure 2A, sorted to show only lineages present on subjects in two families, highlights that lineages on a person often antagonize lineages on other family members. Intensity indicates Area Under the Curve (AUC) for the Zone Of Inhibition (ZOI), and lineages are repeated if present on multiple subjects. (D) Lineages that antagonize a higher fraction of other lineages (red) reach higher abundance on individuals (grey), Spearman's rank correlation.

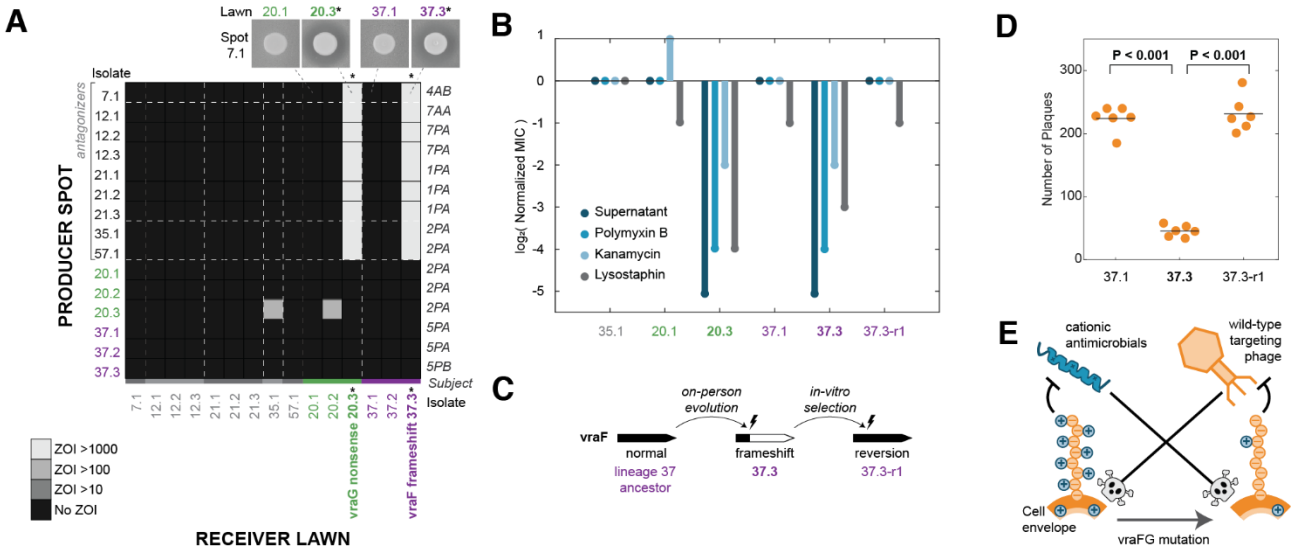

Figure 4: Mutations associated with derived sensitivity to antimicrobials also confer phage resistance. (A) A section of the isolate-level heatmap (from Supplemental Figure 3) filtered to show only a subset of producers and receivers involved in intra-lineage differences. Isolates from the same lineage are indicated by decimals and color. Intensity indicates Area Under the Curve (AUC) for the Zone Of Inhibition (ZOI). Two idiosyncratic isolates (denoted by *) have different sensitivity profiles from the rest of their lineages and also have loss-of-function mutations in the vraFG pathway, as labelled. (B) Isolates with vraFG mutations are sensitive to cationic antimicrobials and lysostaphin. Minimum Inhibitory Concentration (MIC) assay results were normalized to a control isolate (35.1). (C) A frameshift mutation in vraF recently emerged during on-person evolution. By selecting on polymyxin B (Methods), we cultivated revertant isolate 37.3-r1 which corrected the vraF frameshift and has an ancestral resistance profile. (D) Despite other sensitivities, the vraF-frameshift isolate (37.3) was less susceptible to phage infection than isolates with full-length vraF. (E) Together, these results suggest mutations in the vraFG complex reduce cell envelope modifications, weakening resistance to cationic antimicrobials but providing protection against some phage.

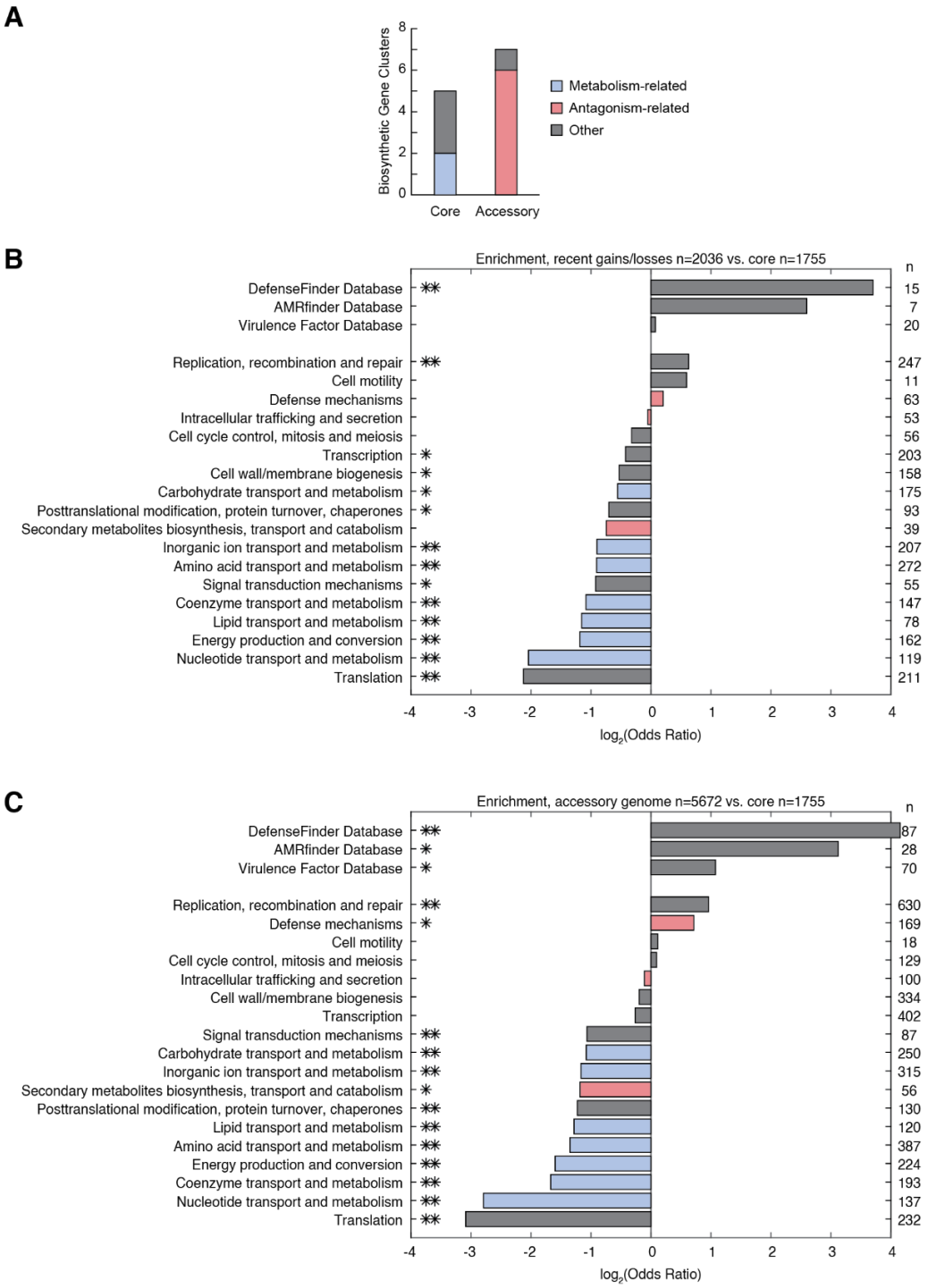

Supplementary Figure 1: Antimicrobial BGCs and defense genes are enriched in accessory genomes. (A) We constructed a pangenome for *S. epidermidis* isolates in our collection and annotated genes and biosynthetic gene clusters (BGCs). Antagonism-related BGCs were more frequent in accessory genomes, whereas metabolism-related BGCs were found in the core genome. (B) We identified regions of the genome with copy number variation within a lineage, indicating recently gained or lost regions. We compared the relative enrichment of COG terms and hits from functional annotation databases among genes in the core genome and recent gain/loss regions. (C) As in B, but comparing genes in the core and accessory genomes. COG categories denoted in blue are metabolism associated, whereas antimicrobial production and resistance genes may be found in red categories. Significant enrichment is indicated by an asterisk (one for naive p-value < 0.05, two for Bonferroni corrected), number of genes annotated in each category is indicated to the right of the figure.

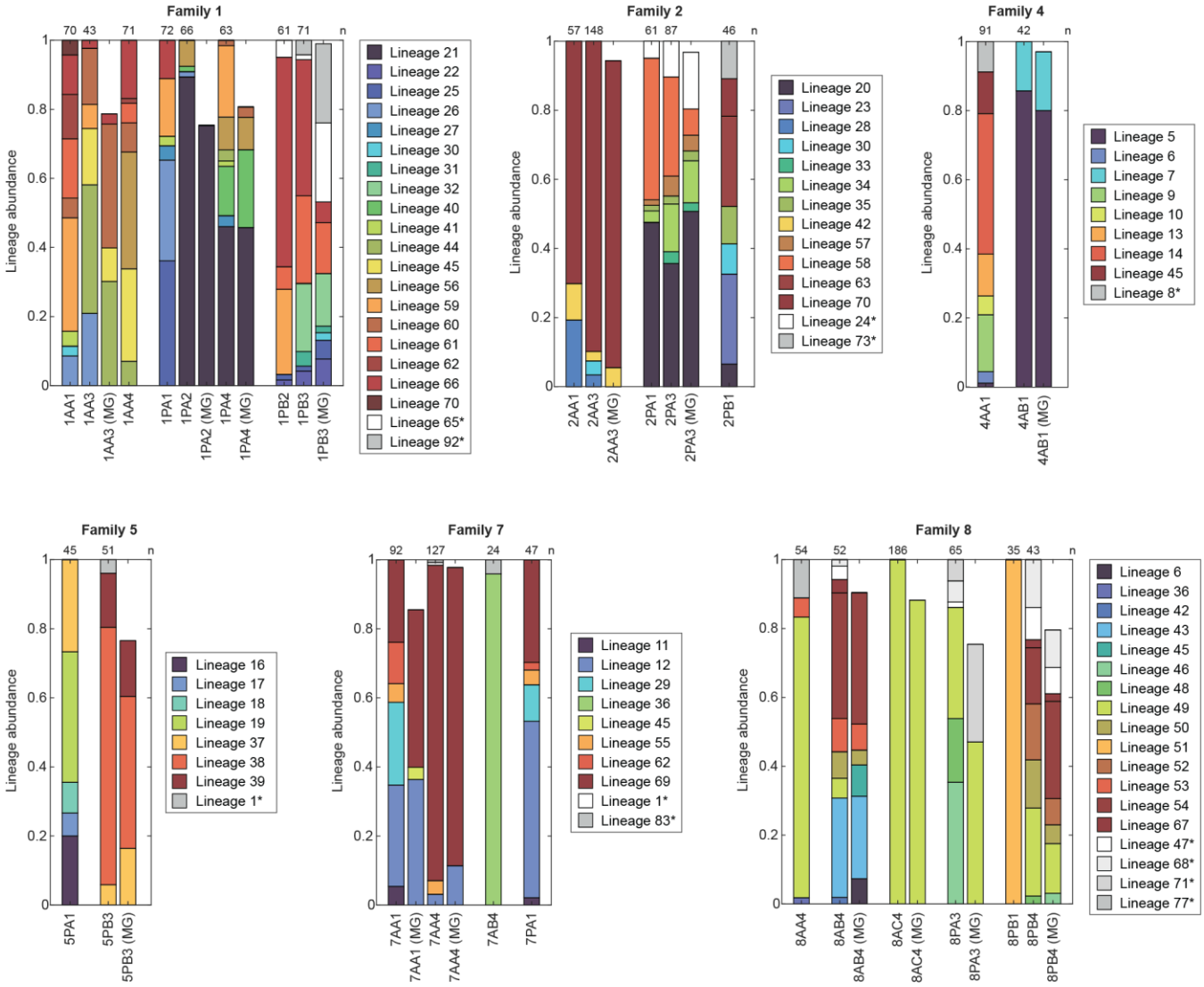

Supplementary Figure 2: Representative isolates capture the *S. epidermidis* lineage diversity of individuals and families. In a previous study, up to 96 isolates of *S. epidermidis* were cultured from each of 23 subjects at each timepoint sampled during a 1.5-year time period. Six families were selected for inclusion in this study. Isolates were chosen to include as many lineages from each sample as possible. Relative lineage abundance, as determined from isolates, is plotted for each sample, organized by subject and family. Sample labels indicate the family, subject, and sampling timepoint, so 1AA3 indicates Family 1, subject 1AA, timepoint 3. The number of *S. epidermidis* colonies isolated from each person is indicated above each bar. Lineages represented in the antagonism screen in this study are indicated in color, while unrepresented lineages (denoted by *) are indicated in greyscale. Across all samples, the average proportion of lineage composition represented by isolates included in the antagonism screen was 96%. Put another way: on average, only 4% of the *S. epidermidis* cells in a sample would not be represented by a lineage included in this study. For samples with sufficient metagenomic coverage of *S. epidermidis* to have 70% of the *S. epidermidis* community predicted at the lineage level, there is good agreement between isolate-inferred abundances and metagenomic-inferred abundances, denoted as (MG). We chose to proceed with isolate-inferred abundances for all analyses because not all samples had sufficiently high metagenomic coverage for *S. epidermidis*.

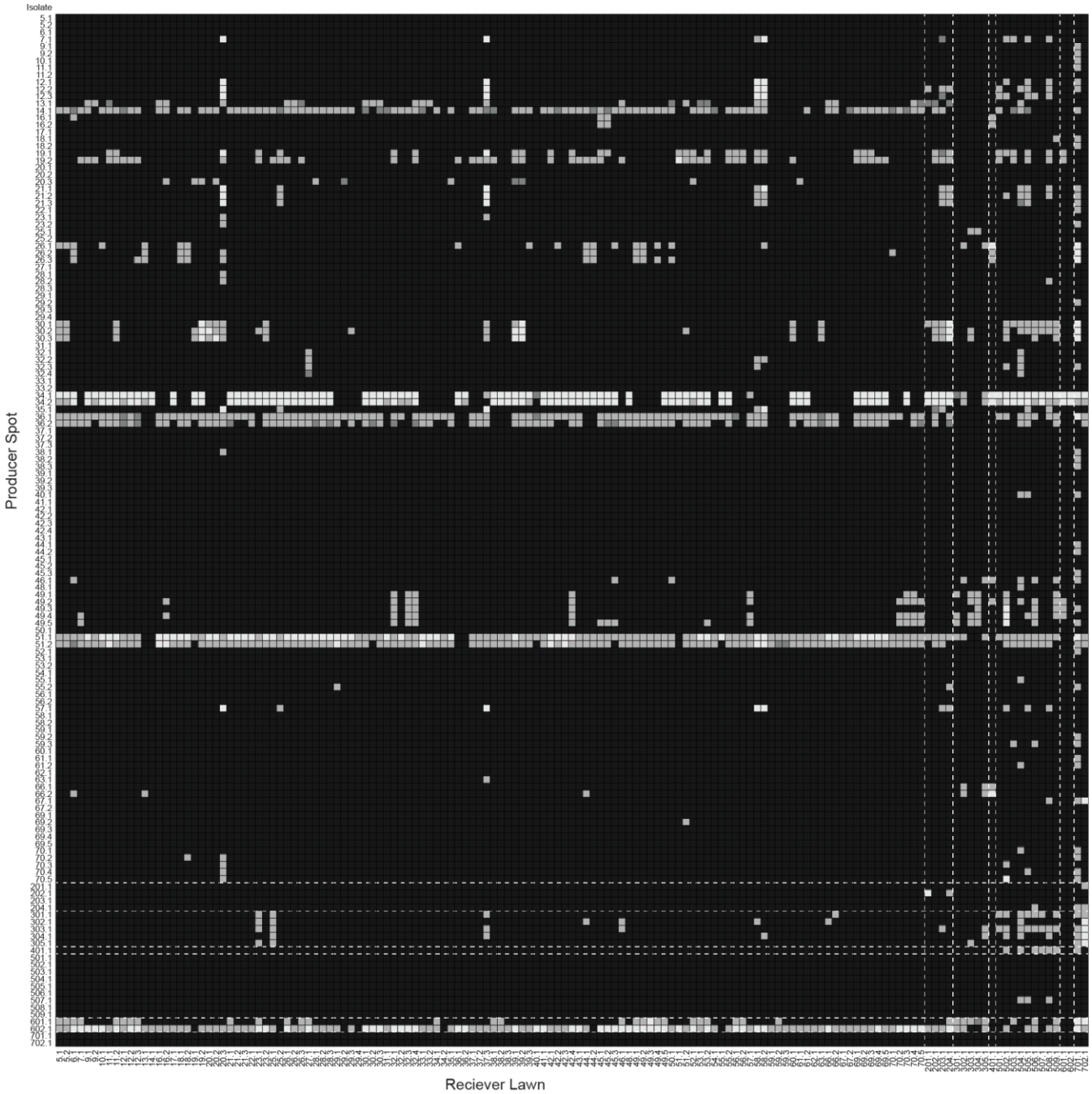

Supplementary Figure 3: Antagonism and sensitivity generally cluster at the lineage level. We measured 21,025 pairwise interactions between 145 isolates that passed inclusion criteria (15 replicate cultures were also included, totaling 25,600 interactions). The heatmap depicts the Area Under the Curve (AUC) for the Zone Of Inhibition (ZOI) calculated for pairwise interactions between *S. epidermidis* and other skin microbiome isolates. Each row and column indicate an isolate (in contrast to Figure 3 where rows indicate lineages). Multiple isolates from a lineage are denoted by decimals (e.g. 20.1, 20.2, 20.3). Isolates are sorted by phylogenetic similarity, with dashed lines to indicate species boundaries. Each isolate of species other than *S. epidermidis* (labels > 200) was treated as a separate lineage. Interactions were shared among all isolates of the same lineage in ~97% of cases.

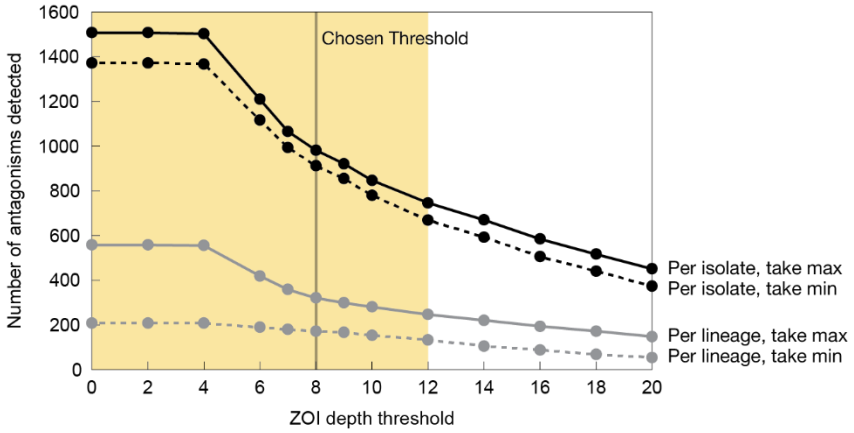

Supplementary Figure 4: Results are robust to alternative choice of thresholds. The threshold cutoffs were chosen to maximize agreement between ZOI calls made by eye vs. by our image analysis pipeline; here we varied the threshold based on ZOI depth, the maximum change in pixel intensity at any radial point surrounding the culture spot. At low and moderate thresholds (yellow), the major results of our study remain significant. However, at more permissive thresholds, the number of ZOIs increases exponentially, potentially indicating spurious ZOI calls. At higher thresholds, legitimate cases of antagonism begin to be excluded and mean antagonism frequency drops low enough that some statistical tests (especially Supplementary Figure 8F) begin to return non-significant results. Separately, the chosen ZOI Depth threshold is approximately the optimum value to minimize the percent difference between two possible lineage dereplication methods (maximizing vs minimizing the number of antagonisms). These findings suggest that our results are not confounded by noisy detection of antagonism or dependent solely on antagonisms of a certain strength.

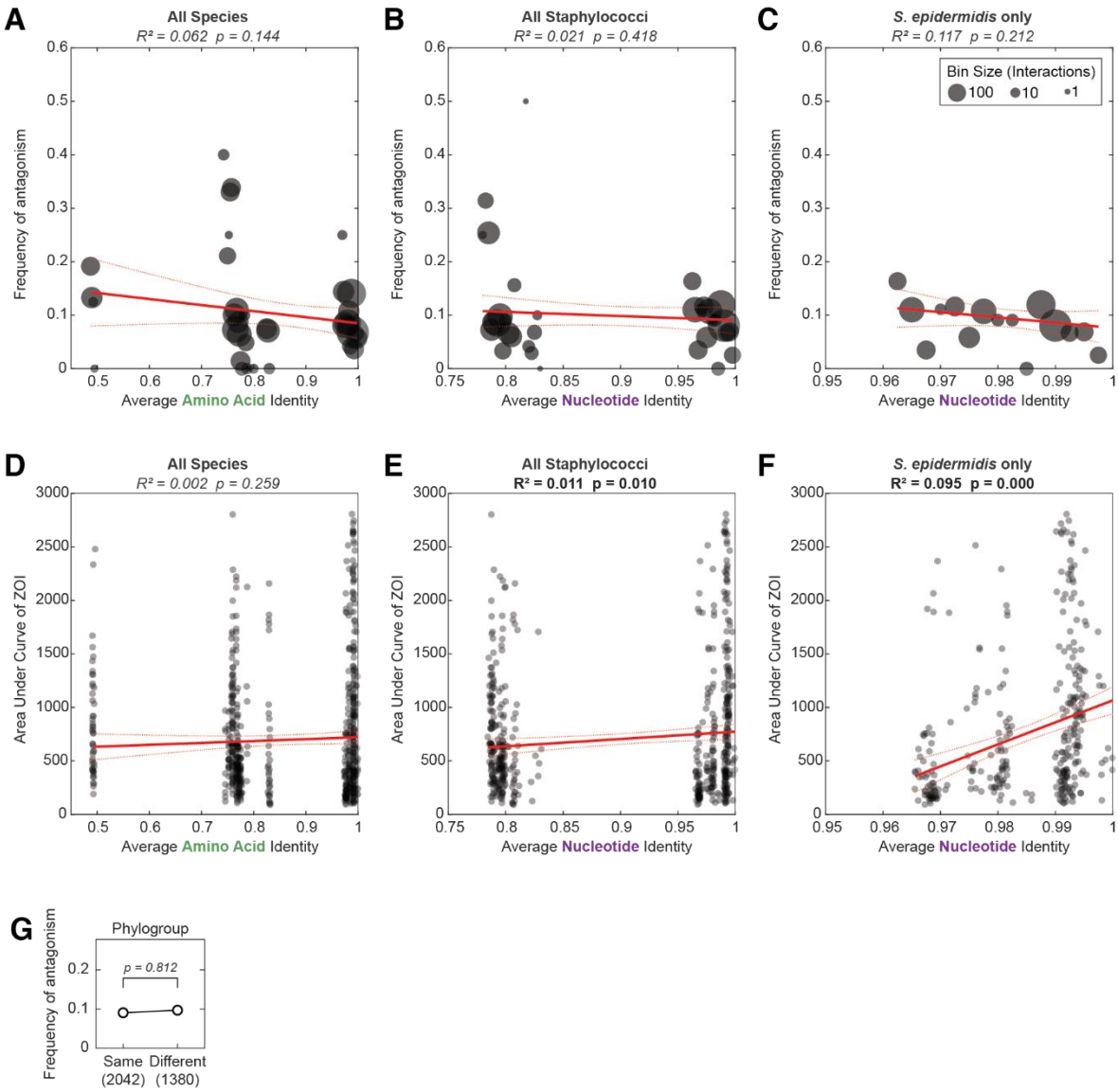

Supplementary Figure 5: Antagonism frequency and strength show limited variation at different phylogenetic distances. Rather than depicting genomic relatedness using a tree (Figure 2), we calculated pairwise distances by different sequence similarities to understand whether antagonism and relatedness are correlated. (A) We binned interactions between pairs of lineages with similar average amino acid identities, then plotted the frequency of antagonism among pairs in each bin. (B) As in A, but binned according to average nucleotide identity. (C) As in B, but only for lineages of *S. epidermidis*, not other species. Antagonism frequency does not significantly vary with genomic distance in our collection, as both R^2 and p are low. (D) We plotted the strength of antagonism (AUC of ZOI) for each antagonistic interaction (excluding non-antagonistic interactions) against the average amino acid identity of the pair. (E) As in D, but against the average nucleotide identity. (F) As in E, but only for lineages of *S. epidermidis*, not other species. There is a significant but small increase in antagonism strength at high nucleotide identities among *S. epidermidis*. (G) The frequency of antagonism does not significantly differ between members of the same or different *S. epidermidis* phylogroup, according to two-sided permutation test with shuffled group labels. Taken together, these results indicate that antagonism occurs at all levels of genomic relatedness, even between closely related lineages.

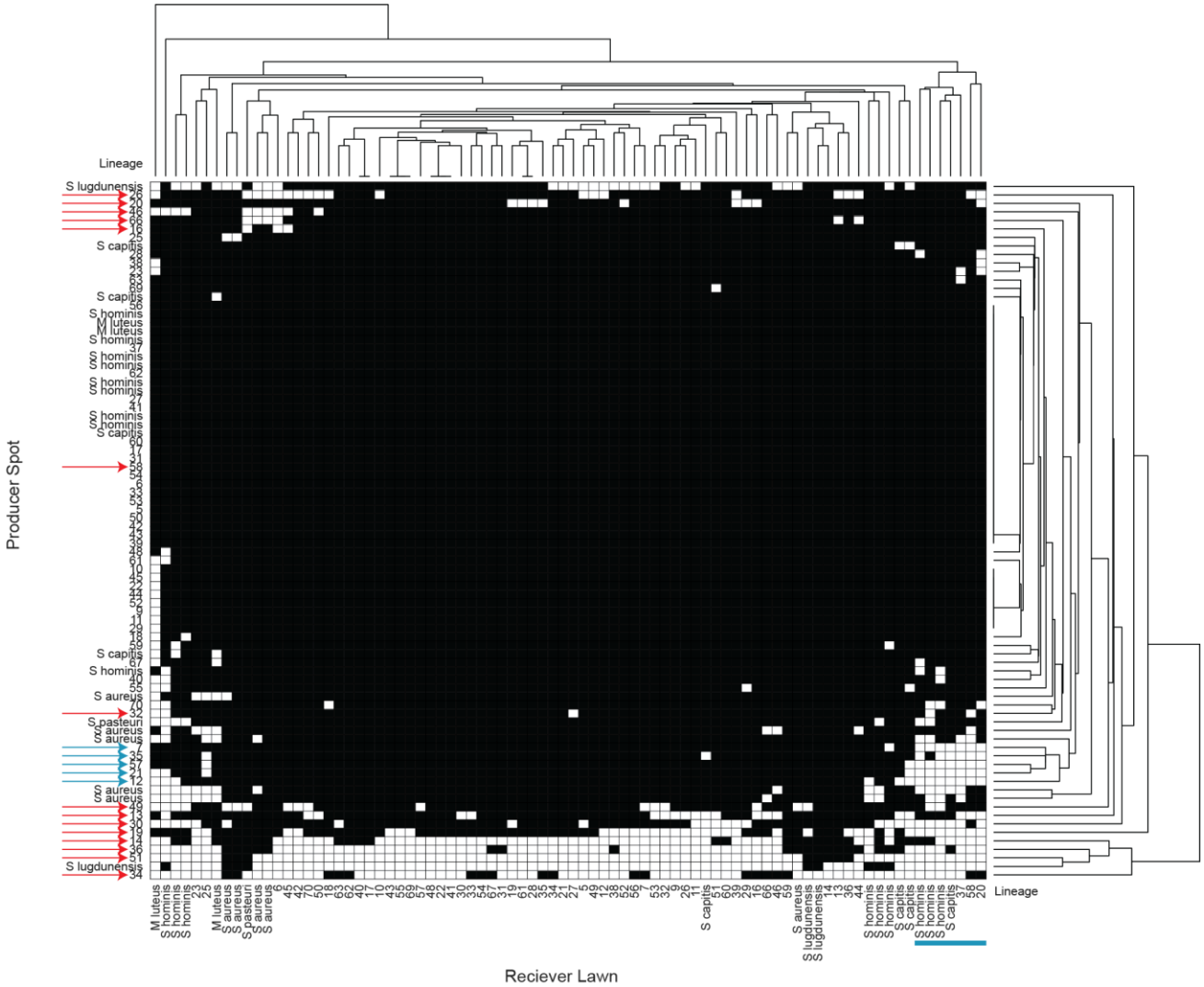

Supplementary Figure 6: Wide variation in intra- and inter-species antagonism patterns. In order to check for shared mechanisms, the binary antagonism matrix was clustered by constructing dendrograms for antagonism and sensitivity. Arrows denote the 18 lineages with high antagonism frequencies (plus 2 with suspected prophage) in our collection that were chosen for our mechanism screen (Supplemental Figure 7). We chose representative receiver bait lineages using the dendrogram of sensitivity to ensure that all interaction patterns were captured. Lineages denoted by cyan arrows did not inhibit many *S. epidermidis*, with the exception of idiosyncratic lineages 20, 37, and 58, which cluster with some *S. hominis* and *S. capitis* isolates, denoted by a cyan line. It is possible that the antimicrobials behind these interactions are intended to target non epidermidis species.

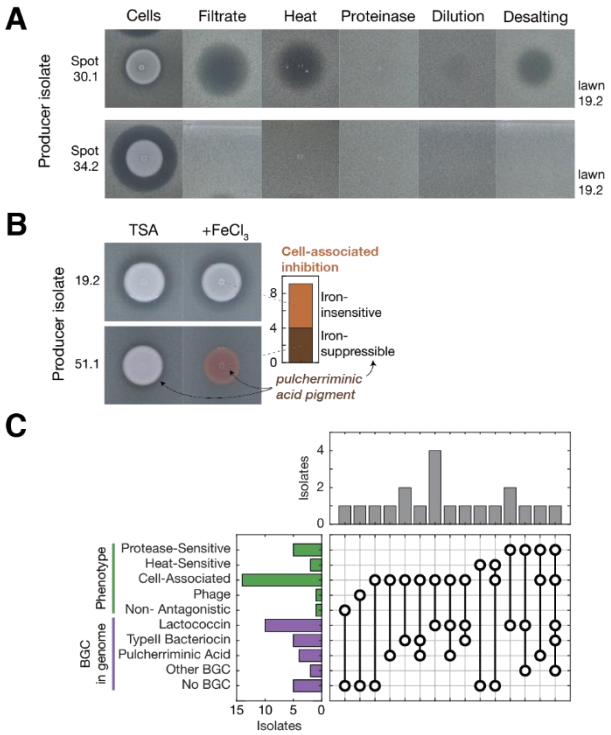

Supplementary Figure 7: Warfare between *S. epidermidis* strains is mediated by diverse and unannotated effectors. (A) To explore the diversity of antagonism mechanisms, we screened cells and filtered supernatants from 20 antagonistic *S. epidermidis* isolates against a representative array of bait lawns chosen based on interaction profiles (Supplementary Figure 5). Filtrates treated with heat or proteinase to degrade proteins and peptides, desalting to remove small molecules, or 1:10 dilution were also tested. Filtrates exhibited varied patterns, including antagonisms likely mediated by small peptide effectors (isolate 30.1) and some cell-associated antagonisms induced by neighbors (isolate 34.2). (B) Some cell-associated antagonisms are iron-mediated, as indicated by the elimination of the interaction in media supplemented with excess $FeCl_3$ (see isolate 51.1). All tested isolates displaying iron-suppressible antagonisms cells contained a biosynthetic gene cluster (BGC) for a product similar to pulcherriminic acid, an iron-sequestering pigment molecule. (C) We annotated putative bacteriocin BGCs but did not find a clear correspondence between BGC presence and the phenotype classified in our mechanism screen, potentially due to multiple inducible effectors being encoded in the genome.

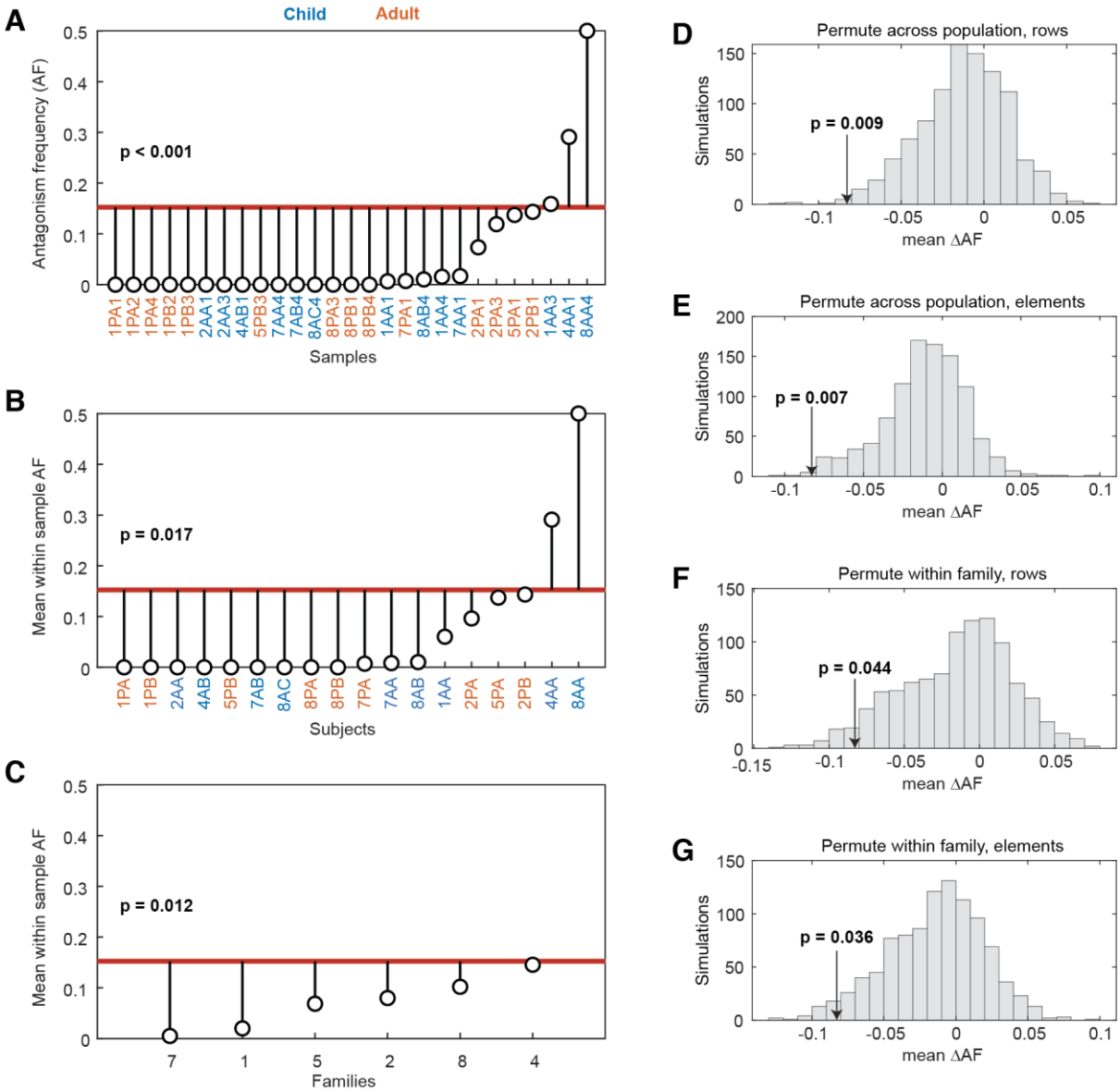

Supplementary Figure 8: Antagonistic interactions are depleted in samples, individuals, and families. (A) Antagonism frequencies (AF) between co-resident lineages in samples is depleted relative to the frequency across all *S. epidermidis* lineages (red), t-test. Subject age groups are denoted as: orange=parent, blue=child. (B) We took the mean AF across samples of the same subject, and still found mean within sample AF to be depleted relative to the expected AF. (C) We took the mean of subjects from the same family, and found mean within sample AF to be depleted relative to the expected AF. Significance p-values derived by 1-sided t-tests, treating samples, subjects, or families as independent. (D) Since t-tests are invalid for non-independent samples, we performed permutation testing by simulating scenarios that retained the structure in the interaction matrix but shuffled lineage labels in the composition matrix. (D) The rows of the composition matrix were shuffled once across all lineages in our collection, so the relatedness between individuals in the same family is retained. (E) The rows of the composition matrix were shuffled once per subject, breaking the relatedness between individuals in the same family. (F) To prevent shuffling across families, submatrices composed only of lineages on a family were shuffled, by row, as in D. (G) Submatrices shuffled but by once per subject. Note that less shuffled conditions (E, F) will definitionally have higher p-values. Under various assumptions, antagonism is depleted among strains present on the same person at the same time.

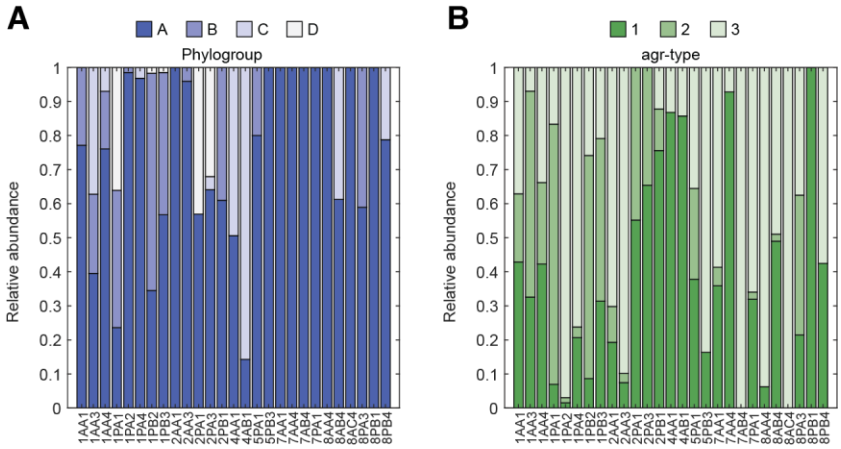

Supplementary Figure 9: Multiple phylogroups and quorum sensing types are coresident on facial skin. (A) Lineages were grouped into phylogroups according to phylogenetic structure as described previously. On many subjects, multiple phylogroups coexist on the face at the same time. (B) The agrD sequence was annotated for each lineage on each subject and classified into quorum sensing types. Again, we found that on many subjects, multiple agr types coexist on the face at the same time. Co-residence between different phylogroups and between incompatible quorum sensing types suggest that there is not competitive exclusion on the basis of phylogenic dissimilarity or quorum sensing.

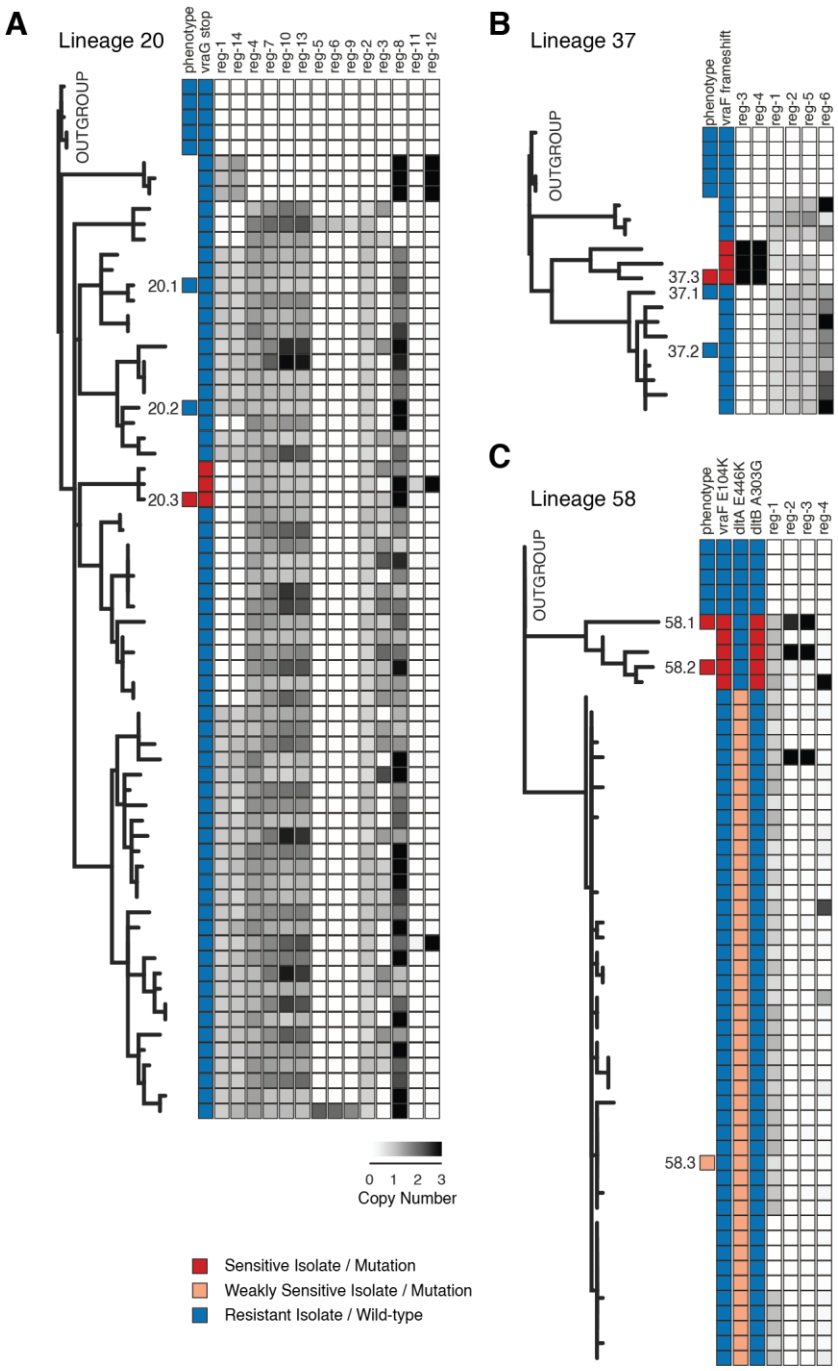

Supplementary Figure 10: Parallel mutations in vraFG pathway in idiosyncratic isolates. To contextualize the results of our mutational analysis, we plotted the idiosyncratic sensitivity phenotype against core genome single nucleotide polymorphism (SNP) trees constructed for each lineage. Each isolate on the tree was annotated with any *vraFG* and *dlt* operon mutations and/or genomic region gains or losses (colored by copy number relative to core genome). The sensitive phenotype (red) correlated with *vraF* and *vraG* mutations in (A) lineage 20, (B) lineage 37, and (C) lineage 58. Presence or absence of genomic regions have no apparent trend in regards to the idiosyncratic sensitivity phenotype. While the *vraFG* mutants form a small fraction of their respective lineages, these isolates were found at multiple timepoints over six months apart, indicating that they are not a transient part of the population.

Isolate	Phenotype	Polymyxin B	Kanamycin	Clindamycin	Ciprofloxacin	Cephalothin	Lysostaphin	Lysozyme	Lauric Acid	Linoleic acid
7.1	antagonist	>256	8	64	0.25	0.25	8	>16	0.25	>16
12.1	antagonist	128	4	0.25	0.25	0.125	8	>16	2	>16
21.2	antagonist	128	8	4	0.5	0.125	32	>16	2	>16
35.1	antagonist	128	4	0.25	0.5	0.125	16	>16	0.5	>16
57.1	antagonist	64	4	2	0.125	0.0625	8	>16	0.5	>16
20.1	wild-type	128	8	4	0.25	0.25	8	>16	0.25	>16
20.2	wild-type	64	8	4	0.25	0.125	16	>16	0.125	>16
20.4	wild-type	128	8	4	0.25	0.125	8	>16	0.5	>16
20.3*	sensitive	8	1	2	0.25	0.0625	1	>16	2	>16
37.1	wild-type	128	4	0.25	0.5	0.25	8	>16	1	>16
37.2	wild-type	64	4	0.25	0.5	0.125	4	>16	1	>16
37.3*	sensitive	8	1	0.25	0.5	0.0625	2	>16	0.125	>16
58.1	sensitive	32	4	0.25	0.25	0.125	16	>16	0.5	>16
58.2	sensitive	16	2	2	0.25	0.0625	8	>16	0.5	>16
58.3	weakly sensitive	32	4	2	0.25	0.125	32	>16	0.5	>16
		µg/mL	µg/mL	µg/mL	µg/mL	µg/mL	µg/mL	µg/mL	mM	mM

MIC Resistant Sensitive

Supplementary Figure 11: Mutations cause correlated sensitivity to cationic antimicrobials and lysostaphin but not to other stresses. Heatmap depicting the Minimum Inhibitory Concentration for antibiotics, lysis enzymes, and antimicrobial fatty acids. Polymyxin B (+5) and kanamycin (+4) are more positively charged than clindamycin (+1), ciprofloxacin (0), or cephalothin (-1). Idiosyncratic isolates 20.3 and 37.3 are more sensitive to cationic antimicrobials and lysostaphin than other isolates in their lineages. Lineage 58 shares a similar sensitivity pattern to these idiosyncratic isolates.

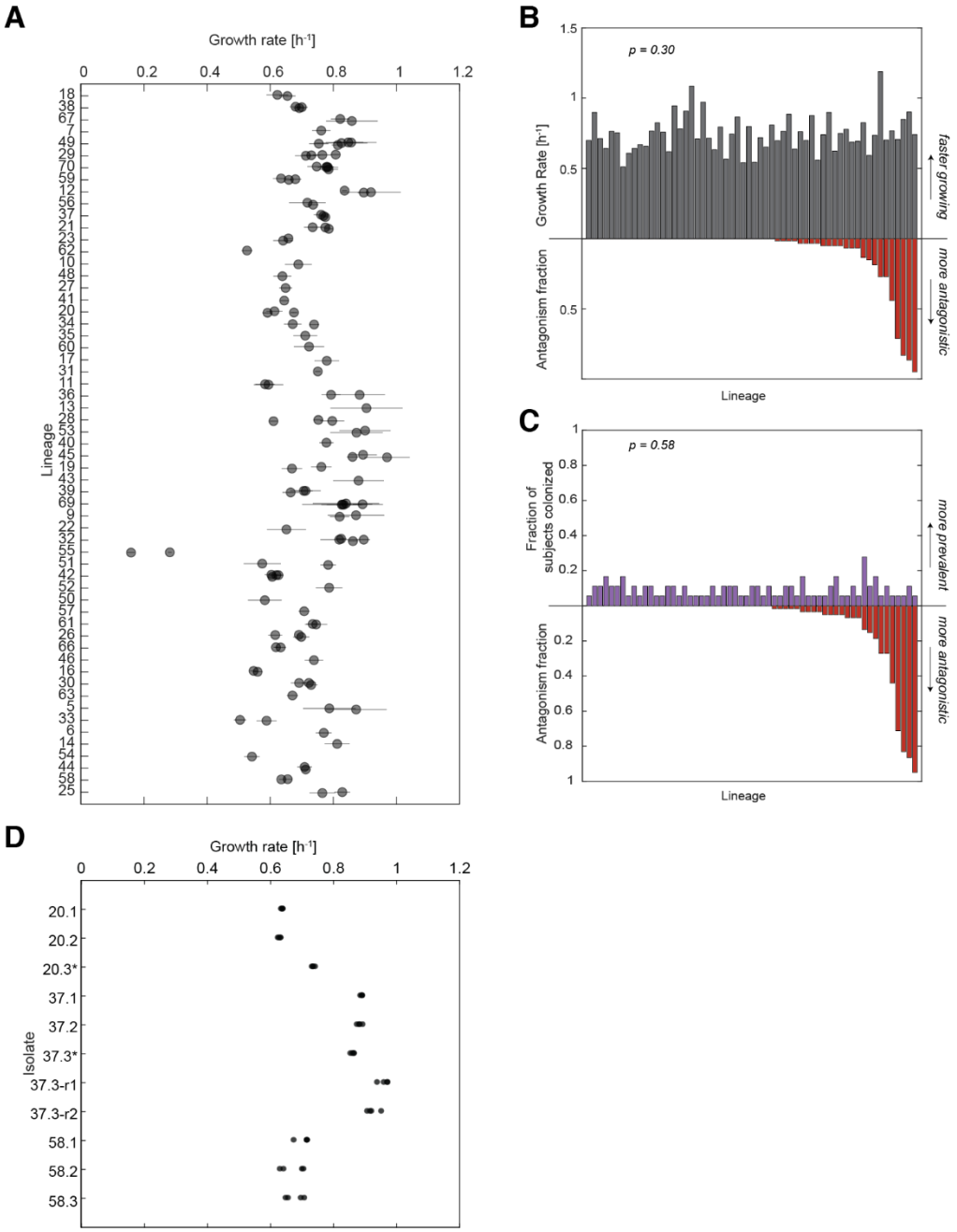

Supplementary Figure 12: Growth rate and fitness variation among *S. epidermidis.* (A) We measured growth rate in liquid shaken plate reader culture for all isolates in our collection. We plotted the median growth rate for each isolate in a lineage (technical duplicates of biological triplicates), bars denote standard deviation. (B) Lineages that antagonize a higher fraction of other lineages (red) do not grow faster or slower than other lineages (grey), Spearman's rank correlation. (C) Lineages that antagonize a higher fraction of other lineages (red) do not colonize more subjects, e.g. they are not more prevalent (purple), Spearman's rank correlation. (D) We plotted the growth rate for each isolate of idiosyncratic lineages 20, 37, and 58 (technical duplicates of biological quadruplicates). Growth rate varies between vraFG mutants and wild-type isolates of each lineage, but without a directional trend.

Methods

Collection and classification of genomically diverse S. epidermidis

Isolates were selected from the collection of *S. epidermidis* created in Baker et al[9]. In that study, 2,025 *S. epidermidis* isolates were clustered into 78 lineages based on core genome single nucleotide polymorphisms. We focused on 6 families chosen because they each had >100 isolates of *S. epidermidis*. In total, 122 representative isolates were selected from each lineage present on subjects from these families. When possible, multiple isolates were chosen from a lineage in order to have isolates from multiple subjects and with different mobile element content. Mobile element content was defined using mapping to lineage co-assemblies as previously described[16]. In addition, 23 isolates from other Staphylococcus species and Micrococcus luteus from these families were also included.

Culture conditions

Unless otherwise noted, all isolates were grown in Tryptic Soy Broth (TSB) (Neogen NCM0004A) aerobically at 37˚C, with shaking at 250 RPM if in liquid culture, or on Tryptic Soy Agar (TSA) with 1.5% agar at 37˚C without shaking if on solid culture. For all experiments, mid-late exponential phase cells were prepared by diluting 5 µL of overnight culture into 495 µL of fresh media and growing these subcultures for 4-6 hours.

Spot-on-lawn assay

Glycerol stocks of single isolates were thawed, then 5 µL of glycerol stock was diluted into 495 µL of fresh TSB + 20% glycerol, arrayed into two 96-well plate arrays (Supplementary Table 1), and aliquoted into 10 µL replicate plates. For each experiment, a replicate plate was thawed; thawed plates were never reused. Overnights were prepared by diluting 5 µL of glycerol aliquot into 495 µL TSB in 2 mL deep-well blocks. Mid-late exponential phase cells were prepared by diluting 5 µL of overnight culture into 495 µL of fresh media and growing these subcultures for 4-6 hours.

For lawn preparation, soft Tryptic Soy Agar with 0.5% agar was autoclaved for 20 mins, then allowed to cool to 55˚C. TSA was then further cooled to 42˚C in a water bath (remining molten). For each lawn isolate, optical density of mid exponential phase cells was measured. Roughly 2.5 x 10^7 cells (adjusted to 0.5 x 10^7 for *S. aureus* to offset higher growth of this species) were added to 50 mL conical tubes along with 35 mL of molten soft TSA. Tubes were mixed by inverting 4 times, then poured into Nunc OmniTrays (Thermo Scientific 242811). Plates were allowed to cool for up to 2 h. While plates cooled, spot cultures were prepared by normalizing the OD of late log-phase sub-cultures to OD 0.1 (roughly 6 x 10^7 CFU/mL) in fresh TSB. A 96-well pipettor (Avidien MicroPro300) was used to dispense 2 µL of spot culture onto each plate. After spots dried (~15 mins), plates were bagged to prevent evaporation and incubated at 37˚C for 24 h then photographed. To more clearly resolve ZOIs by increasing the turbidity of lawn cultures, plates allowed to grow stored at 21˚C for 48 h (to avoid desiccation in the incubator), and photographed again.

Imaging and image analysis

Photographs were taken after 24 h and 72 h of growth. Plates were placed into a custom darkbox with diffuse lighting from the sides and the camera suspended above the plate. Photographs were taken at 6000 x 4000 pixel resolution on a Canon EOS Rebel SL2. Manual focus was determined a single time each day. All images with metadata have been uploaded to figshare (see Data Availability).

Image analysis was performed using a custom MATLAB script applied to greyscale images. Spots, their centers, and their edges were identified as regions of interest (ROIs) centered at 96 points using the imfindcircles function, with any questionable calls flagged for manual ROI definition. The median intensity of pixels for each radial distance from the identified edge was calculated for each spot. These values were corrected for local illumination using the intensity of regions between spots, defined as >180 pixels from any spot center. Spot centers, radii, intensities and variance were stored to allow the user to choose different thresholds to define ZOIs and are available on Github (Supplementary Code). For the results presented here, thresholds were set to an intensity depth of 8 (arbitrary intensity units) and area under the curve (AUC) of 50 (arbitrary intensity units x pixels). Any spots exceeding either of these thresholds were classified as positive. These thresholds were chosen to be conservative and more prone to false negatives than false positives; among replicate spots of the same isolate pairs, ZOIs called in one spot were called only 93% of the time in replicate spots. The major results are robust to alternative threshold choices (Supplementary Figure 4). The dereplicated isolate-level interaction matrix is available in Supplementary Table 4.

When dereplicating isolates into lineages, the maximum ZOI observed between a pair of lineages was chosen as representative. This choice was made due to our conservative ZOI calling pipeline. One case of self-inhibition was overwritten and rescored as non-inhibitory. Calls for plates with poor growth or for spots in areas of glare were masked from subsequent analyses (treated as no data). Ultimately, intra-lineage variation was quantified dividing the number of lineage pairings where isolates disagreed in ZOI call by the number of interactions remaining after first excluding lineage pairs with only one producer or receiver isolate (for antagonism or sensitivity, respectively).

Statistical analysis of antagonism frequency

Weighted antagonism frequency (AF) was defined for each sample (Equation 1), where *f* represents the relative abundance of that lineage in that sample and I_{ij} =1 if lineage i antagonizes lineage j.

$$\text{Equation 1:} \quad AF = \sum_{i,j} f_i f_j I_{ij}$$

To define expected AF across all subjects in our cohort we averaged lineage abundances across all subjects to construct a population abundance vector.

Permutation testing was performed to maintain the structure of interaction matrix while shuffling lineage labels without replacement in a relative abundance matrix (composed of one row for each sample with f_n for every lineage in columns). Shuffling was done in one of two ways that retain the number and balance of lineages on each person: (1) by shuffling columns (retaining correlation between samples from the same person and family or (2) by shuffling elements within rows. Shuffling was performed over either (1) the full relative abundance matrix, or (2) on sub-matrix comprising only lineages present on subjects in the same family. All four combinations of these assumptions were considered (Supplementary Figure 8) and the results were found to be significant to different degrees. Delta Antagonism Frequency (ΔAF) was defined as the difference between the per-sample AF and expected AF calculated from all lineages in our dataset. Mean ΔAF values were calculated for each subject by averaging across samples, and mean ΔAF values were calculated for each family by averaging across subjects. The ΔAF observed in the observed data was compared to ΔAF values generated from 1000 permutation simulations to yield a p-value.

Mechanism screen for antagonistic interactions

Eighteen isolates from the most antagonistic lineages (which each inhibited more than four other lineages) were chosen for mechanistic follow-up. Two other isolates suspected to have active prophages were also included. Hierarchical clustering was performed in order to select 54 representative bait isolates (Supplementary Figure 6). Spot-on-lawn assays were repeated using this representative collection as above, but with five additional supernatant variations for each antagonistic isolate. Supernatant from overnight cultures was passed through 0.22 µm filters (EMDMillipore MSGVS2210), and either applied directly or treated with (a) 3 h incubation with 19 µg/mL proteinase K (GoldBio P-480-SL2), (b) 30 min incubation at 95˚C, (c) column-based desalting (Thermo Scientific 88512), or (d) 1:10 dilution into fresh TSB media. All supernatants were stored overnight at 4˚C prior to spotting on bait lawns. Antagonisms were classified as cell-associated or filtrate-associated depending on whether ZOIs appeared around filtrate spots in addition to cell spots.

To screen for iron-related mechanisms, a third round of spot-on-lawn assays were performed on 11 isolates (to observe 9 cell-associated and 2 filtrate-associated antagonisms). Spot cultures and supernatants (untreated, heat, or proteinase treated) were prepared from cultures pre-grown in TSB or TSA + 90 µM $FeCl_3$ and plated on either soft TSA or soft TSA + 90 µM $FeCl_3$. Pre-growth condition did not alter inhibition phenotypes and filtrate-associated interactions had no altered phenotypes in any condition. Therefore, iron suppression was classified in cases where cell-associated ZOIs on the TSA plate were not observed on the TSA + 90 µM $FeCl_3$ plate.

Identification of putative biosynthetic gene clusters

Published lineage assemblies[9] were annotated using Bakta and screened against specialist databases using AMRFinder[60], VFDB[61], Defense Finder[43]. Cluster of Orthologous Genes (COG terms) were assigned using eggnog-mapper v2[62]. Biosynthetic gene clusters (BGCs) were predicted for each lineage using antiSMASH[63] version 7 with the version 7.0.0 database, and clustered using BiG-SCAPE[64]. All BGCs analyzed are listed in (Supplementary Table 3).

Identification of vraFG mutations in idiosyncratic isolates

Intra-lineage single nucleotide variants (SNVs) phylogenies identified previously[9] were investigated for lineages 20 and 37, which had strong "all-or-nothing" intra-lineage variations in sensitivity (defined as >1000 ZOI AUC range). In addition, Breseq[65] was used to identify for putative insertion-deletion mutations in the same genes as identified SNVs in idiosyncratic isolates. This revealed parallel gene-disrupting mutations identified in vraFG pathway despite there being only 198 SNVs for lineage 20 and 128 SNVs for lineage 37. Lineage 58 carried a similar sensitivity phenotype and had SNVs in the vraG and dltABCDX pathways out of only 78 SNVs. Seeing parallel mutations in this pair of genes across all three lineages is unlikely to happen by chance ($P < 0.0004$, Binomial Test). Tree structures for these lineages indicated derived sensitivity rather than derived resistance (Supplementary Figure 10). This was also found to be true for the two other interactions with intra-lineage ZOI AUC variation >1000 (producer 34 vs. lineage 49 or 70).

Treemaking and distance calculations

Phylogenetic trees were generated in Baker et al[9]. In that study, Widevariant[9] was used to tabulate core genome SNVs without signals of recombination. RaXML v8.2.12 was used to construct a species-wide

maximum parsimony tree from a representative isolate for each lineage and DNApars v3.5c was used to construct a lineage-wide maximum parsimony tree from all isolates of selected lineages.

For computing pairwise distances, an average amino acid identity table was constructed from a representative single assembly from each lineage (for *S. epidermidis*) or species using EzAAI[66]. An average nucleotide identity table was constructed for all Staphylococcus isolates using FastANI[67] from isolate assemblies.

Statistical analysis of antagonism frequency and genomic similarity

We binned interactions by the pairwise amino acid identity or average nucleic acid identity of their corresponding pairs (Supplementary Figure 5) and computed a linear correlation between antagonism frequency or antagonism strength (AUC of ZOI) and genomic similarity. For comparing frequency between categorical groupings, we shuffled species, phylogroup, or agr-type labels in permutation tests (Figure 2). Note that the observed differences would be significant under Fisher's Exact test (e.g. for same vs different species, $P = 0.033$) but due to the structure in the interaction matrix this is a poor assumption, and any differences are negligibly small.

MIC and growth assays

MIC and growth curve assays were performed on sub-cultured log-phase cells diluted to a starting OD of 0.0001. MIC assays were performed in 96-well plates (Greiner BioOne), in 200 µL TSB per well, shaking for 18 h overnight at 37˚C. Growth curves were performed in 150 µL of TSB, grown in a LogPhase600 plate reader (Agilent) at 37˚C, shaking at 800 RPM for 18h, sealed with Breathe-Easy plate seals (Research Products International 248738).

Selection for reversion mutants

Idiosyncratic isolates 20.3 and 37.3 were grown overnight in TSB in 12 replicate 200 µL cultures. Each overnight culture was plated on TSA containing 64 µg/mL of polymyxin B and grown for 24 h at 37˚C. The experiment was repeated a second time for isolate 20.3 using a single 25 mL culture grown in a flask and plating 2 mL per each of 12 plates on 150 mm petri dishes. Resistant colonies 37.3-r1 and 37.3-r2 were grown in TSB 64 µg/mL polymyxin B, and the vraF and vraG sequences were confirmed by Sanger sequencing.

Phage Isolation and Plaque Assay

A 5 mL subculture of *S. epidermidis* isolate 32.1 was grown shaking for 2 h at 37˚C, then mitomycin C was added to a final concentration of 0.8ug/mL. After 6 h of growth, when OD was observed to decrease, cells were pelleted at 2100 x g for 10 mins, and supernatant was filtered using a 0.22 µm filter. To determine plaquing counts, 100 µL diluted filtrates were mixed with 100 µL OD 0.5 subcultures of each *S. epidermidis*, then mixed with 3 mL of 0.5% agar and plated.

Data availability

All sequencing data generated in previous work[9] is available on the NCBI Sequence Read Archive under Bioproject #SUB14054091. All images from the interaction screen are available on Figshare with doi:10.6084/m9.figshare.25726482. All other data is included in the manuscript, supplemental tables, or code base (Code Availability).

Code availability

All code needed to perform the bioinformatic pipeline, image analysis pipeline, and reproduce the figures and analysis in this manuscript is available on GitHub at https://github.com/cpmancuso/Sepidermidis-antagonism.

References

1. Ianiro, G. *et al.* Variability of strain engraftment and predictability of microbiome composition after fecal microbiota transplantation across different diseases. *Nat Med* **28**, 1913–1923 (2022).
2. Caballero-Flores, G., Pickard, J. M., Fukuda, S., Inohara, N. & Núñez, G. An enteric pathogen subverts colonization resistance by evading competition for amino acids in the gut. *Cell Host Microbe* **28**, 526-533.e5 (2020).
3. Watson, A. R. *et al.* Metabolic independence drives gut microbial colonization and resilience in health and disease. *Genome Biology* **24**, 78 (2023).
4. Joglekar, P. *et al.* Integrated genomic and functional analyses of human skin–associated Staphylococcus reveal extensive inter- and intra-species diversity. *Proceedings of the National Academy of Sciences* **120**, e2310585120 (2023).
5. Garud, N. R., Good, B. H., Hallatschek, O. & Pollard, K. S. Evolutionary dynamics of bacteria in the gut microbiome within and across hosts. *PLOS Biology* **17**, e3000102 (2019).
6. Valles-Colomer, M. *et al.* The person-to-person transmission landscape of the gut and oral microbiomes. *Nature* 1–11 (2023) doi:10.1038/s41586-022-05620-1.
7. France, M., Ma, B. & Ravel, J. Persistence and In Vivo Evolution of Vaginal Bacterial Strains over a Multiyear Time Period. *mSystems* **7**, e00893-22 (2022).
8. Oh, J., Byrd, A. L., Park, M., Kong, H. H. & Segre, J. A. Temporal Stability of the Human Skin Microbiome. *Cell* **165**, 854–866 (2016).
9. Baker, J. S. *et al.* Highly-resolved within-species dynamics in the human facial skin microbiome. 2024.01.10.575018 Preprint at https://doi.org/10.1101/2024.01.10.575018 (2024).
10. Dill-McFarland, K. A. *et al.* Close social relationships correlate with human gut microbiota composition. *Sci Rep* **9**, 703 (2019).

11. Koo, H., Hakim, J. A., Crossman, D. K., Lefkowitz, E. J. & Morrow, C. D. Sharing of gut microbial strains between selected individual sets of twins cohabitating for decades. *PLoS One* **14**, e0226111 (2019).

12. Sprockett, D., Fukami, T. & Relman, D. A. Role of priority effects in the early-life assembly of the gut microbiota. *Nat Rev Gastroenterol Hepatol* **15**, 197–205 (2018).

13. Debray, R. *et al.* Priority effects in microbiome assembly. *Nat Rev Microbiol* **20**, 109–121 (2022).

14. Levy, R. & Borenstein, E. Metabolic modeling of species interaction in the human microbiome elucidates community-level assembly rules. *Proceedings of the National Academy of Sciences* **110**, 12804–12809 (2013).

15. Tropini, C., Earle, K. A., Huang, K. C. & Sonnenburg, J. L. The Gut Microbiome: Connecting Spatial Organization to Function. *Cell Host & Microbe* **21**, 433–442 (2017).

16. Conwill, A. *et al.* Anatomy promotes neutral coexistence of strains in the human skin microbiome. *Cell Host & Microbe* **30**, 171-182.e7 (2022).

17. Zeng, M. Y. *et al.* Gut Microbiota-Induced Immunoglobulin G Controls Systemic Infection by Symbiotic Bacteria and Pathogens. *Immunity* **44**, 647–658 (2016).

18. Barroso-Batista, J., Demengeot, J. & Gordo, I. Adaptive immunity increases the pace and predictability of evolutionary change in commensal gut bacteria. *Nature Communications 2015 6:1* **6**, 1–13 (2015).

19. Kitamoto, S. *et al.* Dietary L-serine confers a competitive fitness advantage to Enterobacteriaceae in the inflamed gut. *Nat Microbiol* **5**, 116–125 (2020).

20. Bouslimani, A. *et al.* The impact of skin care products on skin chemistry and microbiome dynamics. *BMC Biol* **17**, 47 (2019).

21. Granato, E. T., Meiller-Legrand, T. A. & Foster, K. R. The Evolution and Ecology of Bacterial Warfare. *Current Biology* **29**, R521–R537 (2019).

22. Riley, M. A. & Gordon, D. M. The ecological role of bacteriocins in bacterial competition. *Trends in Microbiology* **7**, 129–133 (1999).

23. Nakatsuji, T. *et al.* Antimicrobials from human skin commensal bacteria protect against Staphylococcus aureus and are deficient in atopic dermatitis. *Science Translational Medicine* **9**, (2017).

24. Peterson, S. B., Bertolli, S. K. & Mougous, J. D. Interbacterial antagonism: at the center of bacterial life. *Curr Biol* **30**, R1203–R1214 (2020).

25. Coyte, K. Z. *et al.* Horizontal gene transfer and ecological interactions jointly control microbiome stability. *PLOS Biology* **20**, e3001847 (2022).

26. Verster, A. J. *et al.* The Landscape of Type VI Secretion across Human Gut Microbiomes Reveals Its Role in Community Composition. *Cell Host and Microbe* **22**, 411-419.e4 (2017).

27. Ross, B. D. *et al.* Human gut bacteria contain acquired interbacterial defence systems. *Nature* **575**, 224–228 (2019).

28. Vetsigian, K., Jajoo, R. & Kishony, R. Structure and Evolution of Streptomyces Interaction Networks in Soil and In Silico. *PLOS Biology* **9**, e1001184 (2011).

29. Cordero, O. X. *et al.* Ecological populations of bacteria act as socially cohesive units of antibiotic production and resistance. *Science* **337**, 1228–1231 (2012).

30. Russel, J., Røder, H. L., Madsen, J. S., Burmølle, M. & Sørensen, S. J. Antagonism correlates with metabolic similarity in diverse bacteria. *Proceedings of the National Academy of Sciences* **114**, 10684–10688 (2017).

31. Kim, S. G. *et al.* Microbiota-derived lantibiotic restores resistance against vancomycin-resistant Enterococcus. *Nature* **572**, 665–669 (2019).

32. Chesson, P. Mechanisms of Maintenance of Species Diversity. *Annual Review of Ecology and Systematics* **31**, 343–366 (2000).

33. Christensen, G. J. M. *et al.* Antagonism between Staphylococcus epidermidis and Propionibacterium acnes and its genomic basis. *BMC Genomics* **17**, 152–152 (2016).

34. Janek, D., Zipperer, A., Kulik, A., Krismer, B. & Peschel, A. High Frequency and Diversity of Antimicrobial Activities Produced by Nasal Staphylococcus Strains against Bacterial Competitors. *PLOS Pathogens* **12**, e1005812–e1005812 (2016).

35. Lewus, C. B. & Montville, T. J. Detection of bacteriocins produced by lactic acid bacteria. *Journal of Microbiological Methods* **13**, 145–150 (1991).

36. Leyden, J. J., McGinley, K. J., Mills, O. H. & Kligman, A. M. Age-related changes in the resident bacterial flora of the human face. *J Invest Dermatol* **65**, 379–381 (1975).

37. Zhou, W. *et al.* Host-Specific Evolutionary and Transmission Dynamics Shape the Functional Diversification of Staphylococcus epidermidis in Human Skin. *Cell* **180**, 454-470.e18 (2020).

38. Costa, S. K., Cho, J. & Cheung, A. L. GraS Sensory Activity in Staphylococcus epidermidis Is Modulated by the "Guard Loop" of VraG and the ATPase Activity of VraF. *J Bacteriol* **203**, e00178-21.

39. Peschel, A. *et al.* Staphylococcus aureus Resistance to Human Defensins and Evasion of Neutrophil Killing via the Novel Virulence Factor Mprf Is Based on Modification of Membrane Lipids with l-Lysine. *J Exp Med* **193**, 1067–1076 (2001).

40. Peschel, A. *et al.* Inactivation of the dlt operon in Staphylococcus aureus confers sensitivity to defensins, protegrins, and other antimicrobial peptides. *J Biol Chem* **274**, 8405–8410 (1999).

41. Beck, C. *et al.* Wall teichoic acid substitution with glucose governs phage susceptibility of Staphylococcus epidermidis. Preprint at https://doi.org/10.1101/2023.07.27.550822 (2023).

42. Beck, C., Krusche, J., Elsherbini, A. M. A., Du, X. & Peschel, A. Phage susceptibility determinants of the opportunistic pathogen *Staphylococcus epidermidis*. *Current Opinion in Microbiology* **78**, 102434 (2024).

43. Tesson, F. *et al.* Systematic and quantitative view of the antiviral arsenal of prokaryotes. *Nat Commun* **13**, 2561 (2022).

44. Oh, J. *et al.* Biogeography and individuality shape function in the human skin metagenome. *Nature* **514**, 59–64 (2014).

45. Liu, Q. *et al.* Crosstalk between skin microbiota and immune system in health and disease. *Nat Immunol* **24**, 895–898 (2023).

46. Swaney, M. H., Nelsen, A., Sandstrom, S. & Kalan, L. R. Sweat and Sebum Preferences of the Human Skin Microbiota. *Microbiology Spectrum* **11**, e04180-22 (2023).

47. Acosta, E. M. *et al. Bacterial DNA on the Skin Surface Overrepresents the Viable Skin Microbiome*. https://elifesciences.org/reviewed-preprints/87192v1 (2023) doi:10.7554/eLife.87192.1.

48. Sheth, R. U. *et al.* Spatial metagenomic characterization of microbial biogeography in the gut. *Nat Biotechnol* **37**, 877–883 (2019).

49. Mark Welch, J. L., Hasegawa, Y., McNulty, N. P., Gordon, J. I. & Borisy, G. G. Spatial organization of a model 15-member human gut microbiota established in gnotobiotic mice. *Proceedings of the National Academy of Sciences of the United States of America* **114**, E9105–E9114 (2017).

50. Bruce, J. B., West, S. A. & Griffin, A. S. Bacteriocins and the assembly of natural Pseudomonas fluorescens populations. *Journal of Evolutionary Biology* **30**, 352–360 (2017).

51. Claesen, J. *et al.* Cutibacterium Acnes *Antibiotic Production Shapes Niche Competition in the Human Skin Microbiome*. http://biorxiv.org/lookup/doi/10.1101/594010 (2019) doi:10.1101/594010.

52. Wei, M. *et al.* Harnessing diversity and antagonism within the pig skin microbiota to identify novel mediators of colonization resistance to methicillin-resistant Staphylococcus aureus. *mSphere* **8**, e00177-23 (2023).

53. Midorikawa, K. *et al.* Staphylococcus aureus Susceptibility to Innate Antimicrobial Peptides, β-Defensins and CAP18, Expressed by Human Keratinocytes. *Infect Immun* **71**, 3730–3739 (2003).

54. Lai, Y. & Gallo, R. L. AMPed up immunity: how antimicrobial peptides have multiple roles in immune defense. *Trends in Immunology* **30**, 131–141 (2009).

55. Ma, Y. *et al.* Identification of antimicrobial peptides from the human gut microbiome using deep learning. *Nat Biotechnol* **40**, 921–931 (2022).

56. Huang, J. *et al.* Identification of potent antimicrobial peptides via a machine-learning pipeline that mines the entire space of peptide sequences. *Nat. Biomed. Eng* **7**, 797–810 (2023).

57. Maasch, J. R. M. A., Torres, M. D. T., Melo, M. C. R. & de la Fuente-Nunez, C. Molecular de-extinction of ancient antimicrobial peptides enabled by machine learning. *Cell Host & Microbe* **31**, 1260-1274.e6 (2023).

58. Salamzade, R. *et al.* Evolutionary investigations of the biosynthetic diversity in the skin microbiome using lsaBGC. *Microb Genom* **9**, mgen000988 (2023).

59. Shepherd, E. S., Deloache, W. C., Pruss, K. M., Whitaker, W. R. & Sonnenburg, J. L. An exclusive metabolic niche enables strain engraftment in the gut microbiota. *Nature* **557**, 434–438 (2018).

60. Feldgarden, M. *et al.* Validating the AMRFinder Tool and Resistance Gene Database by Using Antimicrobial Resistance Genotype-Phenotype Correlations in a Collection of Isolates. *Antimicrobial Agents and Chemotherapy* **63**, 10.1128/aac.00483-19 (2019).

61. Liu, B., Zheng, D., Zhou, S., Chen, L. & Yang, J. VFDB 2022: a general classification scheme for bacterial virulence factors. *Nucleic Acids Research* **50**, D912–D917 (2022).

62. Cantalapiedra, C. P., Hernández-Plaza, A., Letunic, I., Bork, P. & Huerta-Cepas, J. eggNOG-mapper v2: Functional Annotation, Orthology Assignments, and Domain Prediction at the Metagenomic Scale. *Molecular Biology and Evolution* **38**, 5825–5829 (2021).

63. Blin, K. *et al.* antiSMASH 7.0: new and improved predictions for detection, regulation, chemical structures and visualisation. *Nucleic Acids Res* **51**, W46–W50 (2023).

64. A computational framework to explore large-scale biosynthetic diversity | Nature Chemical Biology. https://www.nature.com/articles/s41589-019-0400-9.

65. Deatherage, D. E. & Barrick, J. E. Identification of mutations in laboratory-evolved microbes from next-generation sequencing data using breseq. *Methods Mol Biol* **1151**, 165–188 (2014).

66. Kim, D., Park, S. & Chun, J. Introducing EzAAI: a pipeline for high throughput calculations of prokaryotic average amino acid identity. *J Microbiol* **59**, 476–480 (2021).

67. Jain, C., Rodriguez-R, L. M., Phillippy, A. M., Konstantinidis, K. T. & Aluru, S. High throughput ANI analysis of 90K prokaryotic genomes reveals clear species boundaries. *Nat Commun* **9**, 5114 (2018).

Acknowledgements

We thank the participants of the original study and C. Dickinson, S. Friedhoff, M. Hirsch, S. Zuckermann, and J. Schuler for assistance with study recruitment. We thank J. Zhou, Z. Zhang, S. Zhang, and S. Levine for advice on experimental design. We thank all members of the Lieberman Lab for advice on this project and feedback on the manuscript.

This work was funded by The James H. Ferry, Jr. Fund for Innovation in Research Education, Colgate-Palmolive Company, and NIH grant 1DP2GM140922 (all to T.D.L).

Author Information

Contributions: C.P.M. and T.D.L. conceived of the project. J.S.B. collected and sequenced the samples. C.P.M., A.D.T., and T.D.L. designed the experiments. C.P.M. carried out the experiments and conducted image processing and statistical analyses. C.P.M., J.S.B., E.Q., A.D.T., and I.O.B. conducted bioinformatic analyses. T.D.L. secured funding for the project. The original manuscript was drafted by C.P.M. and T.D.L.; all authors reviewed and edited the final manuscript.